

Near-Real-Time analysis of the ionospheric response to the 15 January 2022 Hunga Tonga-Hunga Ha'apai volcanic eruption

B. Maletckii¹ and E. Astafyeva¹

¹ Université Paris Cité, Institut de Physique du Globe de Paris (IPGP), CNRS UMR 7154, 35-39
Rue Hélène Brion, 75013 Paris, email : maletckii@ipgp.fr

Corresponding author: Boris Maletckii (maletckii@ipgp.fr)

Key Points:

- We suggest novel methods that detect and characterize ionospheric disturbances due to the Tonga Eruption in the Near-Real-Time (NRT)
- In NRT total electron content time derivative (dTEC/dt), we observe multiple response signatures that indicate multiple eruption scenario
- The peak-to-peak amplitude of the dTEC/dt is comparable to the 2011 Tohoku-Oki earthquake and the 28 October 2003 solar flare

Abstract

We present a near-real-time (NRT) scenario of analysis of ionospheric response to the 15 January 2022 Hunga Tonga-Hunga Ha'apai eruption by using GNSS data. We introduce a new method to determine instantaneous velocities using an interferometric approach and using the time derivative of the total electron content (TEC). Moreover, for the first time, we propose a novel method that automatically estimates the propagation velocity of disturbances from near-real-time travel-time diagrams. By using our new methods, we analyzed the dynamics of co-volcanic ionospheric disturbances generated by the Hunga-Tonga eruption, and we estimated the first propagation velocity to be $\sim 800\text{--}950$ m/s, which subsequently decreased to ~ 600 m/s. We demonstrate that our approach can be used to detect, analyze and identify the complexity of a natural hazard event. Also, it is important to note that our new methods can perform at a low spatial resolution and 30-sec cadence data.

Plain Language Summary

Volcanic eruptions are known to generate strong pressure perturbations that propagate up to the upper atmosphere and generate disturbances in the atmosphere's ionized part - the ionosphere. The 15 January 2022 Hunga Tonga-Hunga Ha'apai submarine volcanic eruption created quite a significant response in the ionosphere. By using a local network of Global Navigation Satellite Systems (GNSS) receivers, we analyze ionospheric response in the near-field area of the volcano. This information can help to complement conventional instruments, since they are not available around the volcano. Therefore, it is important to perform an analysis in near-real-time (NRT). To do so, we introduce novel automatic methods to characterize properties of the response generated by the volcano only by ionospheric GNSS data. These methods suggest the first velocities to be $\sim 800\text{--}900$ m/s, subsequently slowing down to ~ 600 m/s. Besides, our approach allowed us to observe a multi-eruptional scenario.

1 Introduction

It is known that natural hazards, such as earthquakes, tsunamis, and volcanic eruptions generate acoustic and gravity waves that propagate upward in the atmosphere and ionosphere (Astafyeva, 2019). Ionospheric disturbances generated by volcanic eruptions are called co-volcanic ionospheric disturbances (co-VID). It is known that the co-VID are usually quasi-periodically shaped variations that occur ~ 10 to 45 min after the eruption onset, last for 1-1.5 hours, occur in the near field of a volcano (up to ~ 2000 km), with velocities in the range of 0.5 km/s - 1.1 km/s (Heki, 2006; Dautermann et al., 2009; Nakashima et al., 2016; Liu et al., 2017).

Nowadays, we can detect the co-VID by ground-based GNSS receivers. Going further forward, Shults et al. (2016) introduced for the first time a term "Ionospheric Volcanology" that refers to the use of ionospheric measurements for the interests of volcanology. For instance, from the co-VID measurements, it is possible to determine the location of an eruptive volcano, the time of eruption onset (Shults et al., 2016), and estimate volcanic eruption power (Heki, 2006; Dautermann et al., 2009; Manta et al., 2021). Ionospheric-based methods would complement

conventional ones, which use data from nearby seismometers and infrasound stations. The accuracy of those conventional methods decreases in absence of instrumentation within ~100 km from a volcano. To make a step forward toward ionospheric volcano monitoring and warning systems we must develop real or near-real-time (NRT) methods.

In this work, we analyze ionospheric disturbances caused by the 15 January 2022 massive eruption of Hunga Tonga-Hunga Ha'apai (HTHH) volcano. Since the volcano is a submarine one, there are no ground-based instruments nearby, which makes it difficult to calculate the onset time of the eruption. For instance, the US Geological Survey (USGS), <https://earthquake.usgs.gov/earthquakes/eventpage/pt22015050/executive> estimated the onset at 04:14:45 UT, Poli and Shapiro (2022) - at 04:16:00 UT, while satellite data suggest the onset between 04:00 and 04:10 UT. Unreachability of conventional tools makes this eruption a perfect example of when the "Ionospheric Volcanology" could contribute to the. Here, for the first time, we present an NRT scenario of spatio-temporal analysis for this eruption. In addition, also for the first time, we present a new method to determine the co-VID velocity from near-real-time travel-time diagrams (NRT TTD).

2 Data and Methods

Global Navigation Satellite Systems (GNSS) are a helpful tool for ionospheric sounding. Its main advantage is good spatial and temporal resolution. Phase measurements from dual-frequency GNSS receivers allow estimation of the ionospheric total electron content (TEC), which is equal to the number of electrons along a line-of-sight (LOS) between a satellite and a receiver:

$$TEC_{ij} (phase, slant) = \frac{1}{A} \times \frac{f_i^2 f_j^2}{f_i^2 - f_j^2} \times (L_i \lambda_i - L_j \lambda_j) \quad (1)$$

where $A = 40.308 \text{ m}^3/\text{s}^2$, L_i and L_j are phase measurements, λ_i and λ_j are wavelengths at the two the given frequencies (for Global Positioning System (GPS) $i=1, j=2$ and frequencies are 1575.42 and 1227.60 MHz, respectively). The TEC is measured in TEC units (TECu), $1 \text{ TECu} = 10^{16} \text{ electrons/m}^2$.

We use the ionospheric thin shell approximation to calculate the spatial positions of ionospheric disturbances. The intersection points between the LOS and this shell (at a fixed altitude H_{ion}) are ionospheric pierced points (IPP). We use $H_{\text{ion}} = 320 \text{ km}$ since it is close to the maximum ionization height H_mF2 (based on the nearest ionosonde station NIUE at 169.9E; 19.1S).

To study the co-VID signatures driven by the HHTH volcano eruption, we analyze data of 24 ground-based GNSS-receivers in the near-field, i.e., under ~2000 km away from the volcano. To extract the co-VID signatures from the TEC data series, researchers usually apply 1-4 mHz band-pass filters (Heki, 2006; Shults et al., 2016; Nakashima et al., 2016; Manta et al.,

2021). However, in a real-time scenario it is not possible because of the following reasons: a) the impossibility to stack long series of data in NRT; b) such signal properties as arrival time, amplitude, and spectral components can be affected by the filter parameters (Maletckii et al., 2020). For NRT, we propose to use the TEC time derivative, which works as a high-pass filter and removes the bias and trend caused by the satellite orbit motion. In addition, our $d\text{TEC}/dt$ approach will not modify the amplitude of the co-VID.

By using the TEC time derivative approach, Maletckii and Astafyeva (2021a) introduced a method “D1-GNSS-RT” allowing to calculate spatio-temporal properties of traveling ionospheric disturbances (TID) in NRT (Figure 1). To detect TID, the “D1-GNSS-RT” method first analyses TEC data series to find the local maximum value (LMV). Then, it computes the cross-correlation function for each pair of time series around the LMV to calculate the difference in TID arrivals. Finally, based on these time shifts and by using an interferometric approach it estimates the horizontal velocities of TID propagation. The “D1-GNSS-RT” method was tested on several earthquakes but only showed good results with 1-sec data and on dense GNSS networks, such as Japan GEONET. The latter restrictions make it challenging to apply this method to the analysis of the co-VID generated by the HHTH volcanic eruption. The spatial coverage around the Tonga Islands is rather sparse, and only 16 out of 24 GNSS stations provide both 1-sec and 30-sec cadence data, while the others are limited to only 30-sec cadence data (Figure 2a). Besides, 30-sec $d\text{TEC}/dt$ signals have smaller amplitudes and narrower spectral composition, which results in less pronounced signals as compared to 1-sec $d\text{TEC}/dt$ data (Figure S1).

Here, for the first time, we introduce a new “D1-GNSS-RT” applicable to 30-sec data. The main developments are presented in Figure 1. They include: 1) increase of the LMV window to 7 minutes, 2) increase of the cross-correlation window to 24 minutes; 3) decrease of the threshold of the coefficient of the cross-correlation function down to 0.7. However, unfortunately, these new parameters modify the definition of NRT from 15 minutes for 1-sec data to 30 minutes for 30-sec data.

When the “D1-GNSS-RT” is not applicable (e.g., sparse GNSS coverage), the horizontal TID velocity can be estimated by using travel-time diagrams, or hodocrones, that present the TEC variations with respect to the source location and time. Similar to the D1-GNSS-RT, for NRT-TTD we also use the $d\text{TEC}/dt$ parameter. As the source, we take the volcano position. From TTD, the velocity can be estimated as the slope, however, up to now, there was no NRT-compatible automatic method to do that. Here, for the first time, we developed a novel technique to fit the slope line in NRT.

The automatic NRT TTD fitting technique consists of two stages: 1) the first maximum “picker” and 2) the “fitter” based on these maxima.

To select the maximum along with all $d\text{TEC}/dt$ values, we pick the values exceeding a standard deviation of the series and a threshold of 0.15 TECu. In the case of the multiple values in the 120-second windows, we chose the centered one in this window. We also remove outliers from

the final list of maxima in the given series (values that can appear only with velocities exceeding 5 km/s).

We use the first maximum of each data series to fit the first velocity slope. They are sorted based on the source distance - from the closest to the farthest. By analyzing the velocity between the current and previous maximum point we decide whether this maximum is “physically” suitable for the fitting process (velocity between two points should be in the range between 0.1 and 5 km/s and should not vary for more than 20% with respect to the velocity between two previous points; after picking the first 8 suitable maxima we add a new condition - the velocity should not change for more than 50% of the average velocity of all previous points). After the list of suitable points is finished, we fit the slope line by linear regression in these points.

In the case of the Quasi-NRT method, we added a second round for the picking process. After we obtain the first NRT velocity we compare all first maximum velocities with this value. If it lies in a 20% difference border interval, we pick this maximum. The new list of points is used for the Quasi-NRT fitting.

Since the second round would require more time, we call this method “Quasi-NRT”. However, the Quasi-NRT method seems to be more accurate, therefore it can be used to determine NRT-method accuracy in a particular case.

3 Results and Discussion

As shown recently, the explosive eruption of HTHH volcano produced quite a significant response in the ionosphere, and eruption-driven traveling ionospheric disturbances (TID) were observed as far as 20,000 km away from the volcano (Themens et al., 2022; Zhang et. al., 2022). The amplitude of the near-field response reached as high value as 5-8 TECu (Astafyeva E. et. al., 2022). In the case of the dTEC/dt parameter, we observe a peak-to-peak disturbance amplitude of ~8 TECu, which is extraordinary (Figure S2). This value exceeds by a factor of 2.5-3 all previously recorded co-VID (Figure S2). Such large amplitudes were only observed during the 2011 Tohoku-Oki earthquake and during the 28th October 2003 solar flare (Figure S2).

To analyze HTHH-driven response in the NRT scenario, we use our newly developed methods. We estimate spatio-temporal evolution of co-VID, including the amplitude of the velocity, the azimuths of propagation, and the ionospheric source location.

3.1 Spatio-temporal characteristics of the co-VID from D1-GNSS-RT. The instantaneous velocities’ field and source location.

The co-VID velocity field maps for the first arrivals following the Hunga-Tonga eruption are shown in Fig. 2b–d, and the localization results are presented in Fig. 2e–f. Figure 2b shows the first velocity vectors at 04:23:30 UT, i.e., 525s after the eruption onset time, both on the north-east and south-west out from the volcano. From the time of the first co-VID detection, in the NRT scenario, we need 22 minutes more to compute the first velocity field, which is an increase of the time delay for the NRT method as compared to 1-sec data. The two main reasons are a

long 30-sec cross-correlation window (24 minutes vs. 5 minutes with 1-sec data) and sparse spatial resolution. The latter signifies fewer IPP that can be selected for correlation triangles after the first co-VID detection. Therefore, more time is necessary to “form” an interferometric triangle. The first vectors propagate in directions outward from the source. The first horizontal velocities of the co-VID are about $\sim 830\text{--}900$ m/s, i.e., they correspond to acoustic and shock-acoustic waves, and are in line with retrospective studies (e.g., Themens et al., 2022). The first velocity vectors are used to compute the first source location at the point with coordinates (17.90S; 176.26E) (Fig. 2e). The subsequent co-VID evolution during the next 2 minutes maintains the tendency for both the outward direction of propagation and velocities’ values. Further, the velocities decrease to $\sim 500\text{--}600$ m/s, while the source locations concentrate northwest of the volcano (Fig. 2f).

3.2 Spatio-temporal characteristics of the co-VID from NRT TTD using 30-sec data.

The 30-sec NRT-TTD for all satellites and receivers (e.g, all LOS) is shown in Figure 3. From these data, our newly developed method estimates the velocity to be 621.1 km/s. This value is in line with previous retrospective observations for the ionospheric response to the Hunga-Tonga eruption (Themens et al., 2022), as well as with our “D1-GNSS-RT” results. The error of the velocity estimations is less than 10% for both NRT and Quasi-NRT method (Figure 4). The difference between NRT and Quasi-NRT estimations is 11,1%. We can observe the existence of the co-VID signatures before the fitted slope line on Figure 3, but the amplitudes of the disturbances were not sufficient for the “picker” part of the automatic NRT TTD fitting technique.

3.3 Spatio-temporal characteristics of the co-VID from NRT TTD using 1-sec data.

As mentioned above, only 16 GNSS receivers in the near-field of the HTHH volcano provided 1-sec data. This number is too few to use the 1-sec “D1-GNSS-RT” method. However, these limits do not apply to NRT TTD. Figure 5 shows the dTEC/dt-based TTD plotted for co-VID observed in the near-field. We note that the high-rate response to the HTHH volcanic eruption is more complex than the 30-sec one. Figure 5b demonstrates the occurrence of four dTEC/dt disturbances that are, most likely, related to four independent eruptive events that occurred between 04:00 and 05:30 UT. The separate events can be distinguished on TTD based on the characteristics of the ionospheric responses, such as signal shape, the apparent velocity of propagation, and the amplitude.

The NRT TTD shows one quasi-periodic and three N-shaped signatures (dotted ovals in Figure 5b). The first quasi-periodic response (in the green circle) has the lowest velocity along with the others (~ 0.5 km/s). For the second response the slope gives the apparent velocity of ~ 1.33 km/s. It appears to consist of three N-shaped signals which have identical velocity slopes. Further, we distinguish the third event based on a new increase in the dTEC/dt from $\sim 05:15$ UT.

For this component, the velocity slope is ~ 2 km/s. Finally, the fourth event has an apparent velocity of ~ 1.33 km/s, which distinguishes it from the third event, although it is close in time.

Figure 5a shows an example of dTEC/dt signatures for SAMO-R21 (in blue-white-red colormap). We also implement a centered moving average filter (5-sec window) to this series (black curve), which allow to remove noise in data and to concentrate mostly on useful variations. The results prove an assumption of two types of the signatures: first, quasi-periodic and then, N-shaped ones. Evenmore, we observed the first co-VID driven signatures a couple of minutes before USGS determined eruption onset time. Generally, it would need ~ 7 -10 minutes for disturbances to reach the ionospheric altitudes, therefore the eruption onset occurred between 04:00 and 04:10.

Since we observe a difference in the eruption onset time between our results and on-ground techniques, we estimate it based on the slopes and the TTD (Figure 5c). To do so, we first compute the intersection of the velocity slope line with the 0-km distance from the source. Second, we estimate the time in the intersection point from the TTD. This time corresponds to the onset time in the ionosphere, which is the time when the eruption-driven acoustic wave reaches the ionosphere (i.e., the altitude of detection, $H_{\text{ion}} = 320$ km). Third, we compute the vertical propagation time for the acoustic wave from the volcano to the ionosphere by using the sound speed profile derived from the NRLMSISE-2 model (Emmert et al., 2020). With a weighted average velocity of the sound speed of 470 m/s (Figure S3b), the acoustic wave will take ~ 11.34 minutes (11 minutes 20 seconds) to reach 320 km of altitude. Finally, we extract this propagation time from the ionospheric onset times in order to obtain the ground onset times for all four events (Table S1). From our method it follows that the HTHH volcano began to erupt at 04:08:26 UT, which is in agreement with satellite observations that suggest the eruption onset between 04:00 and 04:10 UT (Gusman and Rodger, 2022). Our onset time is also very close to that estimated by Astafyeva et al. (2022) from raw unfiltered TEC data by retrospective analysis. However, it is several minutes earlier than seismically-determined onset time (USGS; Poli & Shapiro, 2022), and ~ 20 minutes earlier than the onset estimated by using a pressure station at Tonga (Wright et al, 2022). Our work demonstrates that our ionosphere-based NRT approach can be successfully used along with conventional methods.

The occurrence of multiple eruptive events, that is clearly seen in dTEC/dt data, is in line with previous reports. For instance, Wright et al. (2022) identified four independent events that occurred between 04:00 and 05:30 UT: 04:26 UT, 04:36 UT, 05:10 UT, 05:51 UT. Astafyeva et al, 2022 suggested the occurrence of five eruptive events between 04:00 and 05:30 UT, however their onset times differ from our estimations since the approximations are different.

4 Conclusions

In this work, we performed for the first time a near-real-time analysis of the ionospheric response to the massive 15 January 2022 Hunga Tonga-Hunga Ha'apai explosive eruption. Our main developments and findings are summarized below:

1. For the first time, we introduce a new method to determine spatio-temporal characteristics in the NRT. This method estimates the instantaneous velocities and the ionospheric source location using not only high-rate data but also the “standard” 30-sec data. In addition, our new method can perform in sparse spatial coverage conditions. We note, however, that 30-sec data increase the NRT time delay between the event onset and the first results to ~30 minutes. By using this method, in a near-real-time scenario applied for the HTHH eruption case, we estimate the first instantaneous velocities to be ~800-900 m/s, which is in line with retrospective studies (e.g., Themens et al., 2022; Zhang et al., 2022), and correspond to acoustic and shock-acoustic waves. The location of the ionospheric source determined by our method is in the northwest of the volcano.
2. For the first time, we present a new method that can estimate the co-VID velocity by using a real-time travel-time diagram. For the HTHH volcanic eruption, we observe the apparent co-VID propagation speed to be 621.1 m/s. This value is in line with our “D1-GNSS-RT” results.
3. Our dTEC/dt NRT-TTD suggest the occurrence of four distinct eruptions between 04:00 and 05:30 UT. From the velocity slopes in NRT-TTD, we estimate the onset time for the four events at 04:08:43 UT, 04:31:00 UT, 05:02:30 UT, and 05:05:21 UT. The multi-eruption scenario is an agreement with the analysis of surface pressure data (Wright et al., 2022) and that of the unfiltered ionosphere TEC data (Astafyeva et al., 2022).
4. We emphasize that the amplitude of the dTEC/dt ionospheric response to the HTHH volcanic eruption is unprecedentedly strong as compared to previously recorded dTEC/dt disturbances. The peak-to-peak dTEC/dt disturbance amplitude exceeded by a factor of 2.5-3 all previously recorded co-VID. According to our knowledge, only two events produced dTEC/dt response with similar magnitude: the 2011 Great Tohoku-Oki earthquake and the 28 October 2003 solar flare.

Our results once again demonstrate the advantages of the use of the dTEC/dt parameter as the effective NRT tool to rapidly determine dynamic characteristics of ionospheric disturbances. We also demonstrate that an ionosphere-based method can be a reliable alternative for detection of natural hazard events. This is especially important and useful for the analysis of submarine events, such as the HTHH volcanic eruption, where ground-based instrumentation is lacking.

Acknowledgments

We thank the French Space Agency (CNES, Project “RealDetect”) for the support. BM additionally thanks the CNES and the IPGP for the Ph.D. fellowship. We acknowledge the use of “tec-suite” codes developed by I. Zhivetiev (<https://tec-suite.readthedocs.io/en/latest/>).

The authors thank Rolland L., Coisson P., Mikesell T. D., Ravanelli M., Munaibari E. and Manta F. for valuable discussion.

Open Research

All GNSS data are available from the CDDIS data archives (<https://cddis.nasa.gov/archive/gnss/data/daily/>).

Ionosonde station NIUE data are available from the DIDBase Web Portal (<https://lgdc.uml.edu/common/DIDBMonthListForYearAndStation?ursiCode=ND61R&year=2022>).

Figures were plotted by using Python (ver. 3.7, libraries “matplotlib.pyplot”: https://matplotlib.org/3.5.0/api/as_gen/matplotlib.pyplot.html and “cartopy”: <https://scitools.org.uk/cartopy/docs/latest/>)

References

1. Astafyeva, E. (2019) Ionospheric detection of natural hazards. *Reviews of Geophysics* 57(4), 1265-1288. [doi.org: 10.1029/2019RG000668](https://doi.org/10.1029/2019RG000668)
2. Astafyeva, E., Maletckii, B., Mikesell, T. D., Munaibari, E., Ravanelli, M., Coisson, P., et al. (2022). The 15 January 2022 Hunga Tonga eruption history as inferred from ionospheric observations. *Geophysical Research Letters*, 49, e2022GL098827. doi.org/10.1029/2022GL098827
3. Dautermann, T., Calais, E., & Mattioli, G. S. (2009). Global Positioning System detection and energy estimation of the ionospheric wave caused by the 13 July 2003 explosion of the Soufrière Hills Volcano, Montserrat. *Journal of Geophysical Research*, 114(B2), B02202. [doi.org: 10.1029/2008JB005722](https://doi.org/10.1029/2008JB005722)
4. Emmert, J. T., Drob, D. P., Picone, J. M., Siskind, D. E., Jones, M., Mlynchak, M. G., et al. (2020). NRLMSISE 2.0: A whole-atmosphere empirical model of temperature and neutral species densities. *Earth and Space Science*, 8, e2020EA001321. <https://doi.org/10.1029/2020EA001321>
5. Gusman, A.R. & Roger, J. (2022). Hunga Tonga - Hunga Ha’apai volcano-induced sea level oscillations and tsunami simulations. GNS Science webpage, [doi.org: 10.21420/DYKJ-RK41](https://doi.org/10.21420/DYKJ-RK41)
6. Heki, K. (2006) Explosion energy of the 2004 eruption of the Asama Volcano, central Japan, inferred from ionospheric disturbances, *Geophys. Res. Lett.*, 33, L14303, [doi: 10.1029/2006GL026249](https://doi.org/10.1029/2006GL026249).
7. Liu, X., Zhang, Q., Shah, M., & Hong, Z. (2017). Atmospheric-ionospheric disturbances following the April 2015 Calbuco volcano from GPS and OMI observations. *Advances in Space Research*, 60 (12), 2836–2846. [doi.org: 10.1016/j.asr.2017.07.007](https://doi.org/10.1016/j.asr.2017.07.007)
8. Maletckii, B., Yasyukevich, Y., & Vesnin, A. (2020). Wave Signatures in Total Electron Content Variations: Filtering Problems. *Remote Sensing*, 12(8), 1340. [doi.org: 10.3390/rs12081340](https://doi.org/10.3390/rs12081340)
9. Maletckii, B. and Astafyeva, E. (2021a) Determining spatio-temporal characteristics of Coseismic Travelling Ionospheric Disturbances (CTID) in near real-time. *Scientific Reports*, 11:20783, [doi: 10.1038/s41598-021-99906-5](https://doi.org/10.1038/s41598-021-99906-5).
10. Maletckii, B. and Astafyeva, E. (2021b) Near-Real-Time Analysis of Spatio-Temporal Characteristics of Ionospheric Disturbances of Different Origins. *Session SA022, AGU Fall Meeting 2021, 13-17 December 2021, Hybrid, New Orleans, USA*
11. Manta, F., G. Occhipinti, E. Hill, A. Perttu, B. Taisne (2021) Correlation Between GNSS-TEC and Eruption Magnitude Supports the Use of Ionospheric Sensing to

- 331 Complement Volcanic Hazard Assessment, J. Geophys. Res. - Solid Earth, [doi:](https://doi.org/10.1029/2020JB020726)
332 [10.1029/2020JB020726](https://doi.org/10.1029/2020JB020726)
- 333 12. Nakashima, Y., Heki, K., Takeo, A., Cahyadi, M. N., Aditiya, A., & Yoshizawa, K.
334 (2016). Atmospheric resonant oscillations by the 2014 eruption of the Kelud volcano,
335 Indonesia, observed with the ionospheric total electron contents and seismic signals.
336 Earth and Planetary Science Letters, 434, 112–116. [doi.org: 10.1016/j.epsl.2015.11.029](https://doi.org/10.1016/j.epsl.2015.11.029)
- 337 13. Noll, C. E. & System, T. C. D. D. I. (2010) A resource to support scientific analysis using
338 space geodesy. Adv. Space Res. 45(12), 1421–1440. [doi.org: 10.1016/j.asr.2010.01.018](https://doi.org/10.1016/j.asr.2010.01.018) .
- 339 14. Poli, P. and M. Shapiro (2022) Rapid characterization of large volcanic eruptions:
340 measuring the impulse of the Hunga Tonga explosion from teleseismic waves. ESSOAr,
341 [doi.org: 10.1002/essoar.10510358.1](https://doi.org/10.1002/essoar.10510358.1)
- 342 15. RTCM. (2020) Radio Technical Commission for Maritime Services.
343 <https://www.rtcn.org/>
- 344 16. Shults, K., E. Astafyeva and S. Adourian (2016). Ionospheric detection and localization
345 of volcano eruptions on the example of the April 2015 Calbuco events. J. Geophys. Res. -
346 Space Physics, V.121, N10, 10,303-10,315, [doi.org: 10.1002/2016JA023382](https://doi.org/10.1002/2016JA023382).
- 347 17. Themens, D. R., Watson, C., Žagar, N., Vasylykevych, S., Elvidge, S., McCaffrey, A., et
348 al. (2022). Global propagation of ionospheric disturbances associated with the 2022
349 Tonga Volcanic Eruption. *Geophysical Research Letters*, 49, e2022GL098158. [doi.org:](https://doi.org/10.1029/2022GL098158)
350 [10.1029/2022GL098158](https://doi.org/10.1029/2022GL098158)
- 351 18. Takasu, T. (2013) RTKLIB: An Open Source Program Package for GNSS Positioning.
352 <http://www.rtklib.com>
- 353 19. Wright, C.J., et al. (2022) Tonga eruption triggered waves propagating globally from
354 surface to edge of space, *ESSOAr*,
355 <https://www.essoar.org/pdfs/10.1002/essoar.10510674.1>
- 356 20. Zhang, S.-R., et al. (2022) 2022 Tonga Volcanic Eruption Induced Global Propagation of
357 Ionospheric Disturbances via Lamb Waves. *Frontiers in Astronomy and Space Sciences*,
358 8, [doi.org: 10.3389/fspas.2022.871275](https://doi.org/10.3389/fspas.2022.871275)

Figures Captions

Figure 1. Scheme of methods developed and implemented in this work. “D1-GNSS-RT” and NRT TTD methods require Real-Time TEC (can be transferred by RTKlib software (Takasu, 2013) and RTCM protocol (RTCM, 2020)) and orbits (can be obtained by Ultra-Rapid Orbits provided by IGS (Noll, 2010)) data. “D1-GNSS-RT” method provides the instantaneous velocities’ field. Based on it, we compute the source location. NRT TTD estimates TID velocity and verifies the link with the source location. The upper part shows the difference in method parameters between the 1-sec “D1-GNSS-RT” and 30-sec “D1-GNSS-RT” that was developed and implemented here for the first time.

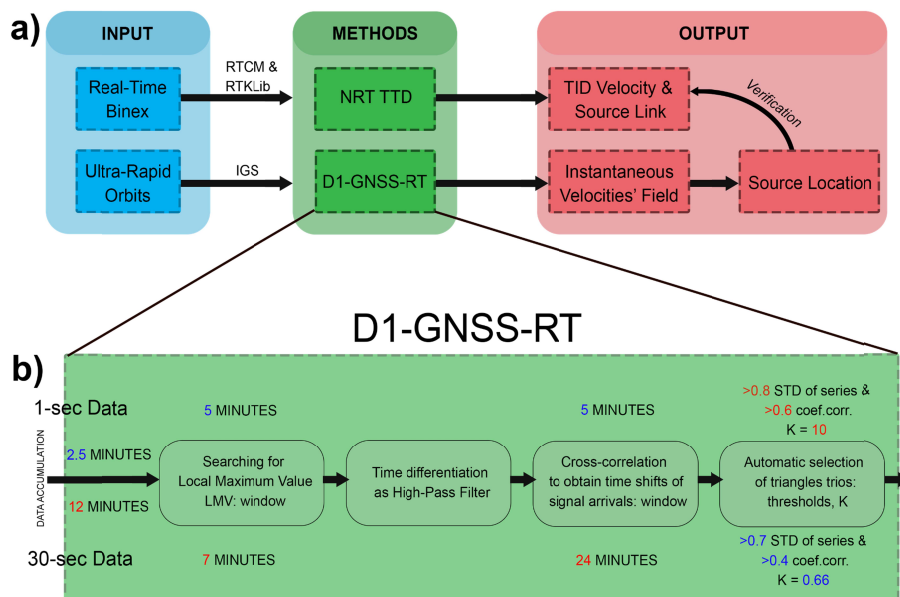


Figure 2. a) The Hunga Tonga-Hunga Ha’apai volcano (red star, 175.382W; 20.53S) and GNSS receivers network used in this work. The receivers that are both sources of 30 sec and 1 sec cadence data: “CKIS”, “FAA1”, “FTNA”, “LAUT”, “PTVL”, “SAMO”, “SOLO”, “THTG”, “TONG”, “TOW2”, “TUVA”, “USP1”. The others provide only 30 second data; **(b-d)** The first instantaneous velocities’ field obtained by “D1-GNSS-RT”. Gray arrow shows the velocity vector of 1000 m/s. The blue arrows correspond to the instantaneous velocities’ field of co-VID; **(e-f)** the source locations obtained from the instantaneous velocities. The blue crosses correspond

379 to the source locations obtained from the instantaneous velocities' field.

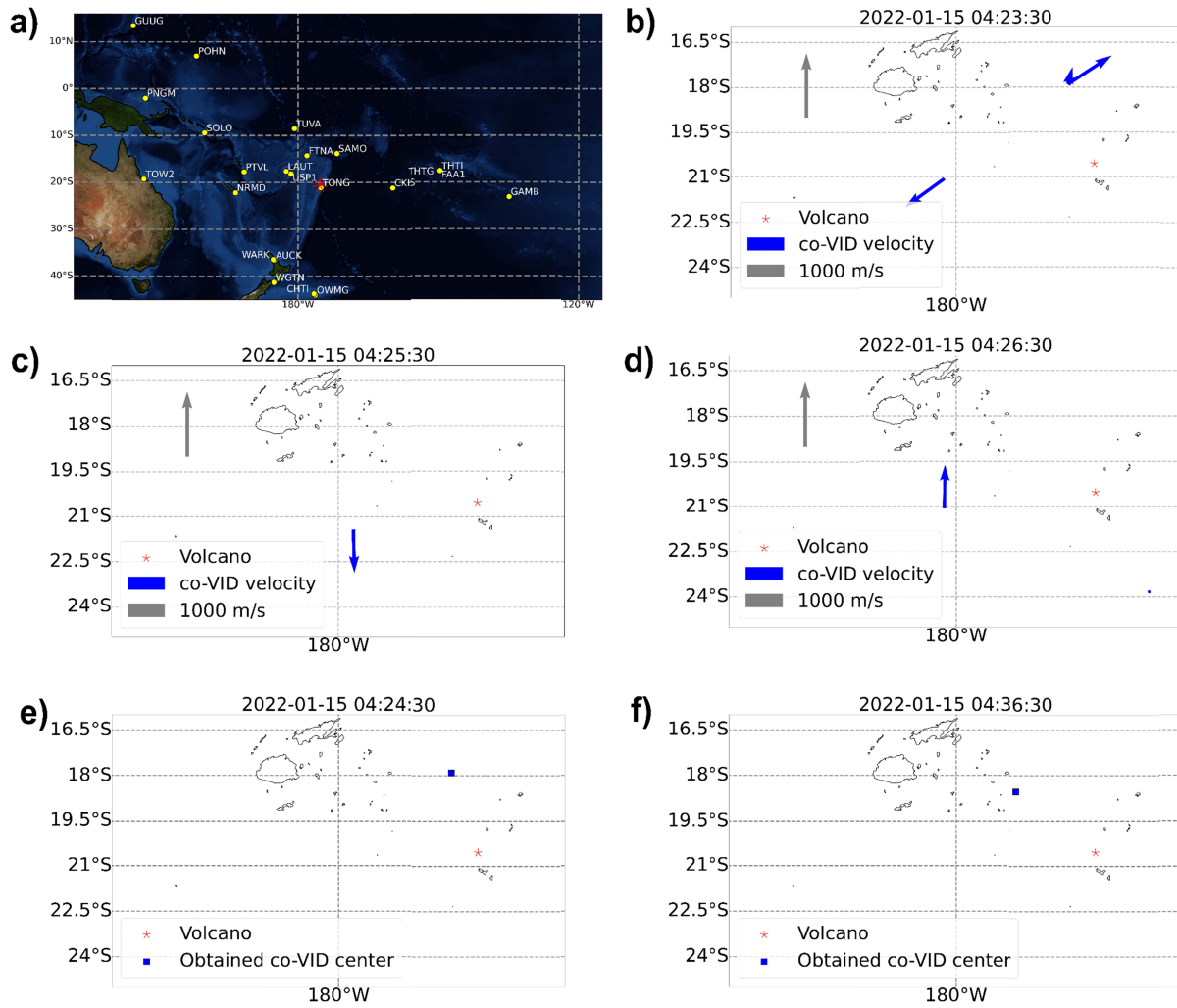


Figure 3. NRT TTD using 30-sec data and co-VID velocity (black line). Gray vertical line shows the USGS onset time. The source is located in the Hunga Tonga-Hunga Ha'apai volcano. The black line was fitted by the newly developed automatic NRT-algorithm.

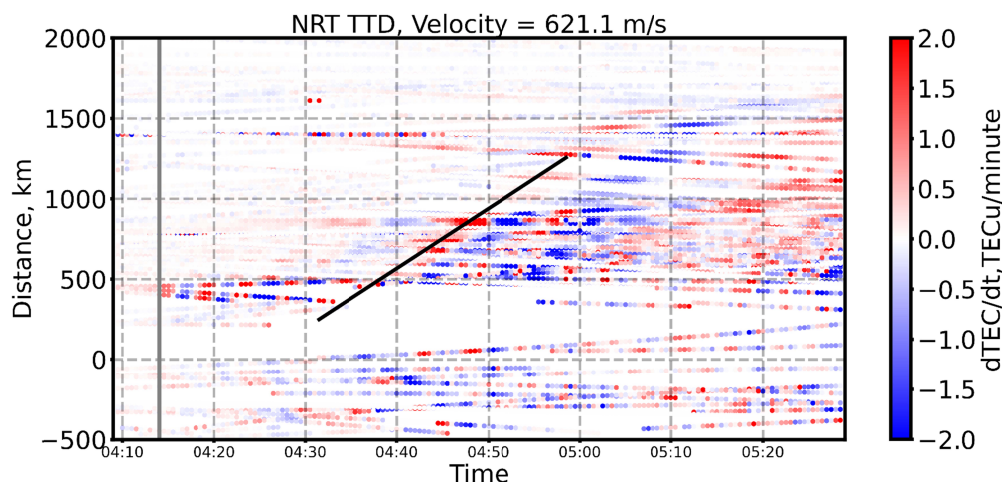


Figure 4. The two fitting algorithms in the TID velocity's slope: (a) the NRT - the brown line, (b) the Quasi-NRT - purple. The blue dots correspond to the first maximums of each series. The red and the green dots are used for the linear regression by the NRT and the Quasi-NRT algorithms, respectively.

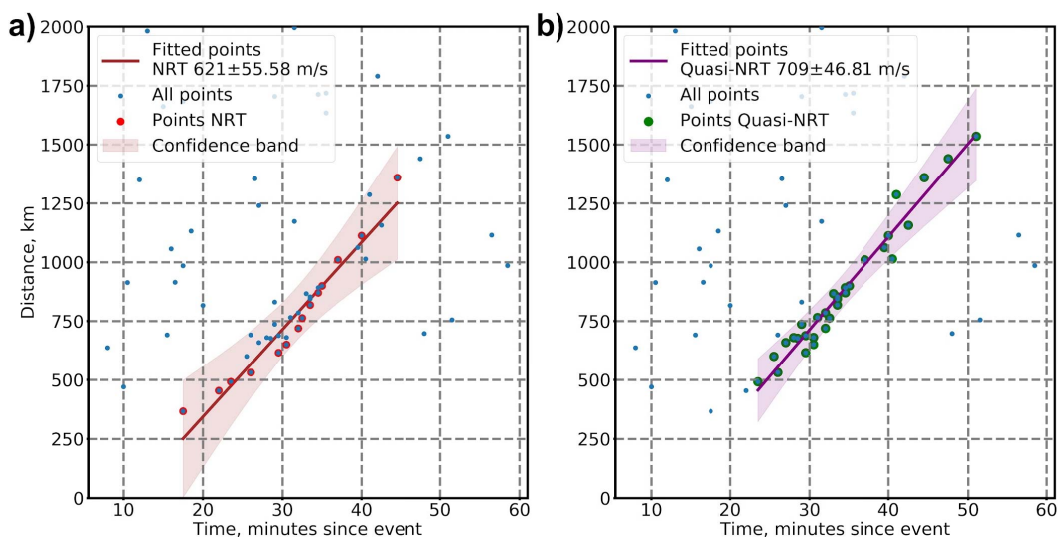


Figure 5. (a) dTEC/dt variations based on the data from receiver SAMO - satellite R21 LOS, blue-white-red curve - 1-sec data, black curve - 5 second centered smoothed data; (b, c) NRT TTD plotted using 1-sec data (b) and (c) zoom on the near-field dTEC/dt response from 04:00 to 05:30 UT. Gray vertical line denotes the USGS onset time, slopes correspond to the independent signatures' velocities, proposed events highlighted in circles (in green - quasi-periodic signature, in dark brown - N-shape ones); (d) schematic representation of multi-eruption scenario and the onset time for each event

